Experimental and theoretical behaviour of reinforced concrete beams containing hybrid fibres

# Experimental and theoretical behaviour of reinforced concrete beams containing hybrid fibres

The corrections made in this section will be reviewed and approved by a journal production editor.

Ibrahim G. Shaaban, Mohamed Said, Sadaqat U. Khan, Mohamed Eissa, Khalifa Elrashidy

University of West London, School of Computing and Engineering, London, Ealing, United Kingdom

## Abstract

The use of fibres of different sizes are needed to improve the control of multi-level cracking of reinforced concrete (RC). There are several studies of the use of hybrid fibres for this purpose, however, there is limited work on the finite element modelling (FEM) of fibres in crack arresting of RC beams. In this study, fifteen RC beams containing silica fume, polyvinyl alcohol (PVA), polypropylene (PP), or hybrid fibres were experimentally tested and then finite element analysis (FEA) was conducted using ATENA 3D. The fibres were used up to 2.5% in the beams which were reinforced with and without shear reinforcement. All the beams were tested under four point bending with span to depth ($a/d$) ratio of 2.25. It was found that the PP, PVA fibres, and their hybrid in RC beams showed higher ductility in terms of multiple cracking before failure as compared with control beam without fibres. It was noticed also that PVA fibre showed a relatively greater flexural strength and recovery effect compared to PP fibre. Adding more than 1.5% PVA or hybrid fibres (1.5% PVA and 0.375% PP) without shear reinforcement contributed towards increasing shear capacity and ductility compared to the control beam containing shear reinforcement without fibres. A combination of small amount of hybrid fibres (0.75% PVA and 0.75% PP) and stirrups reinforcement resulted in a higher shear strength and higher ductility compared to other studied beams without shear reinforcement, which contain PVA, PP fibres up to 2.5% or hybrid fibres (1.5% PVA and 0.375% PP). A simple empirical equation based on the ACI-code 318-19 was used for predicting the shear behaviour of the studied beams taking in to consideration the effect of hybrid fibres for predicting the shear strength of the studied beams in a simple and accurate way. Based on the results of this investigation, it is recommended that a combination of hybrid fibres (0.75% PVA and 0.75% PP) and stirrups reinforcement (7.5 Ø 6 /m) should be used to achieve adequate shear behaviour of hybrid fibre reinforced concrete beams. The FEA results of all beams showed a good correlation with the experimental results in terms of the maximum load, load versus deflection and crack patterns.

**Keywords**: Shear strength; Fibre reinforced concrete beams; Silica fume; PVA fibres; Polypropylene fibres; Hybrid fibres; Finite element

## Nomenclature

$A_s$ the reinforcing area of steel reinforcement bars in tension

$A_{st}$ the reinforcing area of vertical stirrups

$a$ shear-span length

$b$ width of the cross-section

$d$ effective depth of the beam

$d'$ distance from the centre of the tension bars to the concrete tension edge

$E_{ci}$ Modulus of elasticity for concrete

$E_{c0}$ $21.5 \times 10^3$MPa

$E_f$ Modulus of elasticity for PVA and PP fibres

$F_{be}$ bond efficiency of PVA and PP fibres

$f_c'$ cylindrical compressive strength of the concrete

$f_{ck}$ Characteristic compressive strength of concrete in MPa based on cylindrical compressive strength.

ft Tensile strength, MPa

$f_y$ yield strength of the longitudinal steel reinforcement bars

$f_{y,st}$ yield strength of the vertical stirrups

$l_f$ length of PVA and PP fibres

$t$ depth of the cross-section

$P_{u,\ \exp}$ experimental ultimate load

$\delta_{u,\ \exp}$ experimentally measured ultimate deflection

$S$ spacing between the vertical stirrups

$V_a$ the aggregate interlock action

$V_c$ contribution of concrete to the shear resistance

$V_{cc}$ resistance of the compressed concrete

$V_d$ dowel action of the longitudinal bars

$V_{u,\ Anl.}$ predicted ultimate shear strength

$V_{u,\ \exp.}$ experimental ultimate shear strength

$V_{fibres}$ shear resistance of PVA fibres and PP fibres

$V_s$ shear resistance of vertical stirrups

$V_f$ volume of fibres

$\propto_E$ 1.0 for quartzite aggregates

σt Tensile stress

$\rho_f$ percent by volume of PVA and PP fibres

$\phi_f$ diameter of PVA and PP fibres

## 1 Introduction

Concrete is the most in abundance used material in the world after water. Due to good compressive behaviour, it has been widely used building material, while poor tension properties are covered using steel bars as reinforcement. Although steel bars enable concrete to withstand against almost all types of loads and provide the ductility to structural members, it has some drawbacks such as controlling cracks and penetration of ingress substances that may cause corrosion of steel [1]. Dispersed fibre reinforcement offers secondary reinforcement to concrete as bridges for stress-transfer [2] to solve those problems. Adding fibres to the concrete matrix can enhance concrete's flexural strength and post-cracking properties, which enhance concrete's ability to resist cracking. Fibres are divided into three groups according to their size: microfibers, macro fibres and Meso fibres [3]. Generally, microfibres are 6 to 20 mm in length, and tens of microns in diameter. These were commonly accepted as an important way of managing plastic shrinkage. However, because microfibres are small, if structures reach the large-deformation zone, they give little structural benefits for concrete. Besides, macro fibres, usually 30 to 60 mm long and more than 0.3 mm in diameter, are capable of bearing loads and preventing the propagation of visible cracks after concrete matrix breaks, such as steel bar reinforcement [1]. Meso-fibres, on the other hand, are smaller than macro fibres but larger than microfibres and are capable of bridging the cracks from the micro level to macro level up to some extent [3]. As can be shown, there is no single form of fibre that can provide all-round strength, ductility, and resilience and thus combining various fibre sizes are required to control multi-level cracking of reinforced concrete [4–6].

Asok and George [7] investigated the mechanical properties of hybrid steel Polypropylene (PP) fibre concrete using 1% and 0.035% volume fractions of hooked end steel and monofilament polypropylene fibres. The results showed that the compressive, tensile splitting and flexural strengths of hybrid steel-PP FRC were obtained higher than the plain concrete. Sukontasukkul [8] investigated the tensile response of FRC containing steel and PP fibres as alone and as a hybrid system by utilizing 1 to 5% volume fractions. The outcome of the study [8] revealed that the behaviour of FRC using steel fibres was typical, i.e., the peak of the load occurred at a minimal deformation and was shadowed by the fall of the load to zero without any sign of the load recovery. Furthermore, the behaviour of FRC incorporating PP fibres was more ductile as compared to the steel fibres alone. It showed a typical double-peak response, i.e., the first peak occurred at a small deformation, and the second peak occurred at the large deformation. Li, Biao, et al. [9] investigated the flexural behaviour of hybrid FRC using the steel-PP combination in which three types of steel fibres (straight, hooked-end, and corrugated fibre, and monofilament PP fibres. The results showed a synergetic influence using a combination of PP fibres with all the three types of steel fibres in improving flexural behaviour. Apart from the studies [7–11], Hou et al. [12] investigated the effects of temperature and stress on the creep behaviour of hybrid reactive powder concrete using PP and steel fibres. In literature, the use of steel and PP fibres together is preferable to obtain higher strength and avoid shrinkage cracking.

Smarzewski [13] investigated the flexural toughness high-performance concrete (HPC) hybrid reinforced with basalt/PP fibres with proportions of 0/0, 100/0, 75/25, 50/50, 25/75, and 0/100% by volume at total volume fractions of 1 and 2%. It was found that 50/50 and 100% PP fibres only gave the best results in terms of flexural toughness of HPC. In another study [14], the mechanical properties of HPC with basalt and PP fibres were investigated. It was found that the flexural and splitting tensile strength were improved. The optimised content for the best mechanical performance was found to be 0.15% of basalt fibres and 0.033% of PP fibres. Yan, Chen et al. [15] investigated the micro-size basalt, PP and glass fibres dosage of 0.5%, 1.0%, 1.5%, 2.0%, and 2.5% of volumetric fractions in ultra-high performance concrete (UHPC). It was observed that the fresh properties were less affected with the addition of PP fibres, whereas, the compressive strength was increased with 0.5% of fibres and was decreased with the increase in fibre volume. The modulus of rupture and toughness index were increased and found comparable with these fibres.

Pakravan et al. [16] studied the effect of combining polyvinyl alcohol (PVA) and PP fibres in different ratios on the flexural behaviour of cementitious composite concrete (ECC) beams. The ratios of PVA / PP fibres (75/25%, 50/50%, 100/0% and 0/100%) at different fibre volume fraction contents (1.2% and 2%) were considered as the variables. The results showed that the fibres increased the flexural strength and ductility of cement matrix while hybrid fibres (PVA and PP) had a little effect on flexural strength. In addition, the replacement of PVA fibre with 25% volume fraction of PP fibres improved the ductility of ECC. Pakravan et al. [17] in another study investigated the effect of hybrid PP with PVA fibres, on the structural behaviour of Engineered Cementitious Composites (ECC) concrete elements including fly ash as cement replacement material. The flexural behaviours of the ECC concrete elements containing hybrid fibres including first-crack strength, post-crack strength, and toughness were studied under three-point bending test. The results indicated that partially replacement of PVA fibres with non-round cross-sectional shape PP fibres improved the ductility and it could be considered to be promising method to reduce the costs of ECC production along with attaining improved deformability. Feng et al. [18] studied the compressive and flexural strength of hybrid fibre reinforced concrete containing fly ash. The experimental results showed that the combination of PVA, PP, and steel fibres resulted in improving compressive and flexural strength. It was found also that the impact toughness of SF-PP hybrid fibre reinforced concrete as well as Steel-PVA hybrid fibre reinforced concrete was significantly improved due to the positive hybrid effect of these combinations. Ismail and Hassan [19] studied the shear behaviour of large-scale engineered cementitious composite (ECC) concrete beams containing fly ash and reinforced with a combination of steel, PP and PVA fibres of different lengths. The ultimate capacity and cracking moment of all the test beams were compared with theoretical values estimated by some design code equations. They found that the cracking behaviour, shear capacity, ductility, and energy absorption of the ECC beams are higher than those of NC beam. The ECC beam reinforced with PVA (8 mm) fibres showed the highest shear strength and ductility of all the ECC beams with other polymeric fibres. The beam reinforced with PP (19 mm) showed the lowest performance, while the use of steel fibres (13 mm) proved to be the most effective in improving the first crack load, ultimate load, ductility and energy absorption capacity.

This overview presents the extent of investigations performed to date on using a hybrid combination of fibres. PP fibre has low Young's modulus, which results in less effective reinforcement than steel fibres [1]. The use of basalt fibres and PP fibres are promising, however, the results are not as good as the combination of steel and PP fibres. On the other hand, the use of steel fibres also have concerns such as higher thermal conductivity [20], low fire resistance [21], tire puncture hazards in pavements, and corrosion of fibre close to the concrete surface [22]. The use of PP and PVA fibres in concrete and cementitious composites found beneficial, however, there is a need to investigate the structural behaviour of reinforced concrete beams with the hybrid use of PP and PVA fibres.

This study is focusing to use PP and PVA fibres in reinforced concrete beams designed to be fail in shear. Fifteen fibre reinforced concrete beams containing silica fume, shear span to depth ($a/d$) ratio of 2.25 and different percentages of PVA (0–2.5%), PP (0–2.5%), and hybrid fibres (0.375%, and 0.75%) were experimentally tested. The provided fibre content of PVA, PP, and hybrid fibres was on the basics of the conducted previous studies [1–12,20]. Adding hybrid fibres aims to enhance the ductility of the studied beams while the utilisation of silica fume aims to enhance the strength and durability (compressive strength ranged from 53 to 58 MPa after 28 days water curing). The experimental results were further confirmed by finite element modelling of these beams.

## 2 Preparation, Details and testing of beam specimens

A grade 52.5 Portland cement was supplied by a local factory, compatible with European standards (2004/1-197EN) [23]. The silica fume was supplied by Sika Egypt for Construction Chemicals Complying with ASTM C 1240 [24] (see Fig. 1). The physical and chemical properties of silica fume are described in Table 1. Concrete specimens are reinforced with different volume percentages of PVA and PP fibres where their properties are listed in Table 2 and the shape of the fibres is shown in Fig. 2 (a) and (b). A polycarboxylic High Range Water Reducer (HRWR) from BASF Construction Chemicals (Master Glenium RMC 315) complying with EN934-2 [25] was used. The quantities required by weight for one cubic meter of fresh concrete for the specimens are given in Table 3. Concrete was cast in the wooden forms, including reinforcing steel cages, just after mixing as shown in Fig. 3. Since the width of beam was less than the depth, all the beams were cast from the side rather from the top to make sure good compaction as shown in Fig. 4. The concrete was cast and vibrated with an electrical needle vibrator and the final concrete surface was smoothened as shown in Fig. 4. The forms were removed after 24 h from casting and specimens were exposed to moisture continuously with water for 28 days in laboratory atmosphere until they were tested. Concrete cubes and cylinders along with the beam specimens were cast from each mix and they were water cured to obtain the actual cube compressive strength on the day of testing. The consistency of fresh concrete was measured by a slump test according to EN 12350-2 [26]. Based on the results of the slump test, the slump classes EN 206-1 (2006) [27] reported in Table 4 show that the slump of the fibrous concrete ranged between 160 and 200 mm (class S4) whereas normal concrete showed a slump of 140 mm (class S3). This is due to the increase in HRWR supplied for the fibrous mixes. The cube compressive strength results are

reported in Table 4, whereas, the cylindrical compressive strength and stress–strain parameters were used for FEM analysis and will be discussed in the forthcoming section.

**Fig 1**

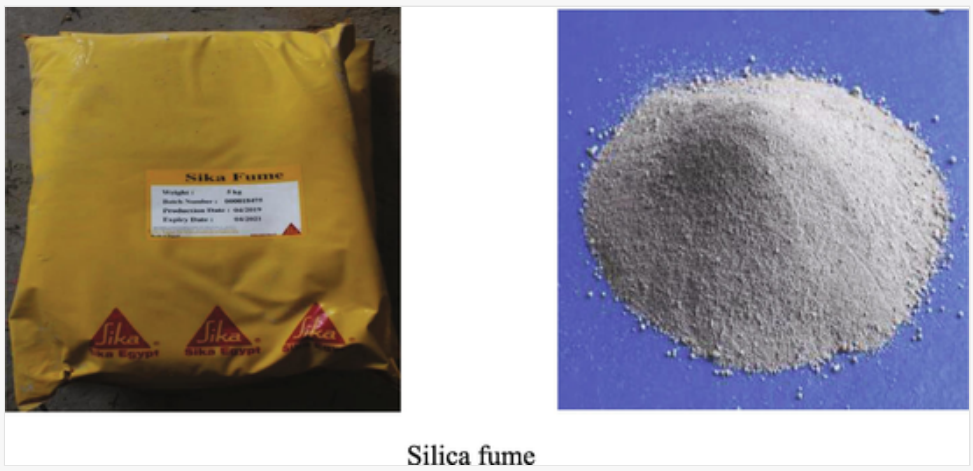


Cement replacement materials used in this investigation.

**Table 1**

The table layout displayed in this section is not how it will appear in the final version. The representation below is solely purposed for providing corrections to the table. To preview the actual presentation of the table, please view the Proof.

Properties of the used silica fume.

| | |
|---|---|
| SiO2 | >88.9% |
| Moisture | <0.57% |
| Alkalis like Na2O | <0.5% |
| Free CaO | <0.1% |
| Free SI | 0.14% |
| Free Cl% | 0.02% |
| SO3 | <0.25% |
| L.O.I (incl. carbon) | <4.5% |
| Specific surface | ~20 $m^2$/gr |
| Size | ~0.15microns |

**Table 2**

The table layout displayed in this section is not how it will appear in the final version. The representation below is solely purposed for providing corrections to the table. To preview the actual presentation of the table, please view the Proof.

Properties of the Polyvinyl Alcohol (PVA) and Polypropylene (PP) fibers.

| Type | Length (*lf*) (mm) | Shape | Diameter ($\phi f$) (mm) | Tensile Strength (MPa) | Elastic Modulus(GPa) | Density($\rho$)(g/$cm^3$) | Elongation (%) |
|---|---|---|---|---|---|---|---|
| PVA | 12 | Monofilament | 0.039 | 1620 | 42.80 | 1.3 | 7.0 |
| PP | 12 | Monofilament | 0.018 | 400 | 3.45 | 0.91 | 80 |

**Fig 2**

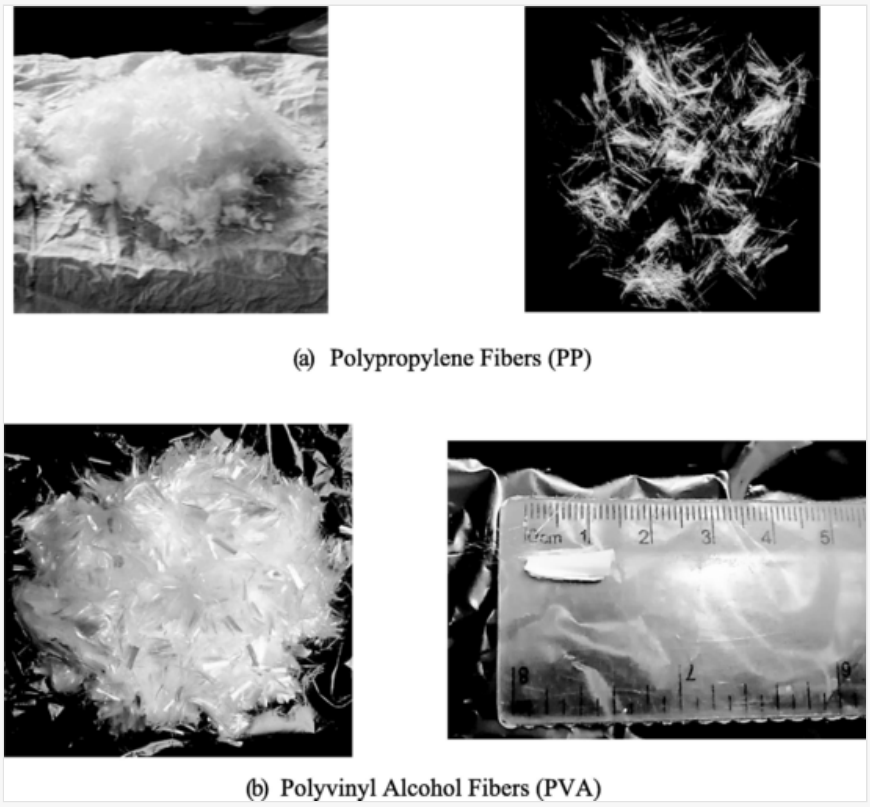


Short fibres used in the concrete mixes.

**Table 3**

The table layout displayed in this section is not how it will appear in the final version. The representation below is solely purposed for providing corrections to the table. To preview the actual presentation of the table, please view the Proof.

Mix proportions for concrete mixes (kg/m$^3$).

| Mix | Cement | Silica fume | Fine Sand | Coarse Aggregate | Water | PP Fiber | | PVA Fiber | | HRWR |
|---|---|---|---|---|---|---|---|---|---|---|
| | | | | | | kg | % | kg | % | |
| MIX 1 | 425 | 75 | 620 | 1180 | 181 | 0 | 0.0 | 0 | 0.0 | 8 |
| MIX 2 | 425 | 75 | 620 | 1180 | 179 | 0.0 | 0.0 | 10 | 0.75 | 10 |
| MIX 3 | 425 | 75 | 620 | 1180 | 177 | 0.0 | 0.0 | 20 | 1.5 | 12 |
| MIX 4 | 425 | 75 | 620 | 1180 | 175 | 0.0 | 0.0 | 33 | 2.5 | 14 |
| MIX 5 | 425 | 75 | 620 | 1180 | 177 | 14.25 | 1.5 | 0.0 | 0.0 | 12 |
| MIX 6 | 425 | 75 | 620 | 1180 | 175 | 23.75 | 2.5 | 0.0 | 0.0 | 14 |
| MIX 7 | 425 | 75 | 620 | 1180 | 179 | 7.35 | 0.75 | 0.0 | 0.0 | 10 |
| MIX 8 | 425 | 75 | 620 | 1180 | 180 | 3.56 | 0.375 | 5 | 0.375 | 9 |
| MIX 9 | 425 | 75 | 620 | 1180 | 179 | 7.35 | 0.75 | 10 | 0.75 | 10 |
| MIX 10 | 425 | 75 | 620 | 1180 | 177 | 3.56 | 0.375 | 20 | 1.5 | 12 |

**Fig 3**

Mixing the concrete mixes mechanically.

**Fig 4**

Rendering and smoothening the final concrete surface.

Table 4

The table layout displayed in this section is not how it will appear in the final version. The representation below is solely purposed for providing corrections to the table. To preview the actual presentation of the table, please view the Proof.

Average mechanical properties of fresh and hardened concrete.

| Mix | 1 | 2 | 3 | 4 | 5 | 6 | 7 | 8 | 9 | 10 |
|---|---|---|---|---|---|---|---|---|---|---|
| Specific Gravity (kg/m$^3$) | 2420 | 2430 | 2435 | 2440 | 2480 | 2435 | 2440 | 2425 | 2480 | 2480 |
| Air Content (%) | 5.8 | 5.6 | 5.3 | 5.2 | 5.7 | 5.5 | 5.6 | 5.7 | 5.8 | 5.8 |
| Slump Class | S3 | S4 | S4 | S4 | S4 | S4 | S4 | S4 | S4 | S4 |
| Cube Compressive Strength (MPa) at 28 days | 56 | 54 | 57 | 58 | 54 | 54 | 53 | 57 | 58 | 57 |

The performed experimental work consisted of fifteen large-scale beams of span (L) = 1800 mm, depth (t) = 300 mm, effective depth (d) = 260 mm and width (b) = 120 mm, were simply supported and tested under the effect of two concentrated loads (see Fig. 5). The test beams represented four Groups A, B, C and D as indicated in Table 5. The steel bars were tied with the stirrups forming reinforcement cages corresponding to that require for connections as shown in Fig. 6. The beams were over reinforced in flexure in order to obtain shear failure. Electrical strain gauges of 10 mms length and 120.3 ± 0.5-ohm resistance were fixed on the steel bars, with the position shown in Fig. 5, in order to follow the reinforcement strains during loading. The strain gauges were covered with silicon sealant to protect them during casting and consolidation of concrete. The electrical strain gauges were coupled to a strain indictor. The test specimens were instrumented to measure their deformational behaviour after each load increment and the test setup is shown in Fig. 7. The recorded measurements included also concrete, lateral deflection, and crack propagation. The deflections were measured using 3 Linear Variable Displacement Transducers (LVDT) 100 mm capacity and 0.01 mm accuracy and arranged to measure the deflection distribution to the specimen as shown in Fig. 5. After each load increment, the cracks were traced and marked on the painted sides of the specimen.

**Fig 5**

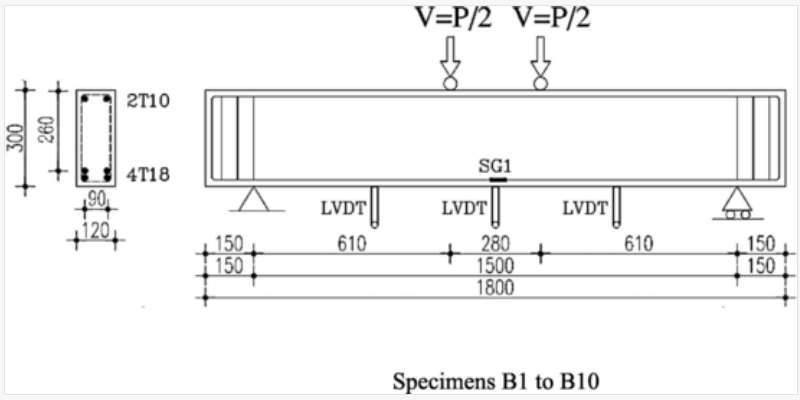


Position of demec points, electrical strain gauges, and LVDTs for a typical beam.

**Table 5**

The table layout displayed in this section is not how it will appear in the final version. The representation below is solely purposed for providing corrections to the table. To preview the actual presentation of the table, please view the Proof.

Details of the tested beams.

| Group | Mix | Beam | Shear span to depth ratio (a/d) | Fiber content (PVA) Vf % | Fiber content (PP) Vf % | Stirrups / m |
|---|---|---|---|---|---|---|
| A | MIX 1 | B1 | 2.25 | 0 | 0 | – |
| | MIX 2 | B2 | | 0.75 | 0 | – |
| | MIX 3 | B3 | | 1.5 | 0 | – |
| | MIX 4 | B4 | | 2.5 | 0 | – |
| B | MIX 5 | B5 | 2.25 | 0 | 1.5 | – |
| | MIX 6 | B6 | | 0 | 2.5 | – |
| | MIX 7 | B7 | | 0 | 0.75 | – |
| C | MIX 8 | B8 | 2.25 | 0.375 | 0.375 | – |
| | MIX 9 | B9 | | 0.75 | 0.75 | – |
| | MIX 10 | B10 | | 1.5 | 0.375 | – |
| D | MIX 1 | B11 | 2.25 | 0 | 0 | 7.5 Ø 6 / m |
| | MIX 8 | B12 | | 0.375 | 0.375 | |
| | MIX 9 | B13 | | 0.75 | 0.75 | |
| | MIX 3 | B14 | | 1.5 | 0 | |
| | MIX 4 | B15 | | 2.5 | 0 | |

**Fig 6**

Beams with no stirrups

Beams with stirrups 7.5 Ø 6 /m

Steel reinforcement cages for typical specimens.

**Fig 7**


Test setup for a typical beam.

# 3 Experimental results and discussion

## 3.1 Load-Deflection Results, crack Patterns, and failure mode shapes

Fig. 8 (a-d) show the load deflection relationships for the test specimens comprising the four studied groups mentioned in Table 5. Fig. 8 (a-d) show that the load displacement curves for all the test specimens exhibited similar pattern for the different studied beams but with different ultimate loads and corresponding deflections, based on the PVA%, PP%, hybrid fibres%, and presence of stirrups. Fig. 9 (a-d) show the crack pattern and failure modes of all the test beams.

**Fig 8**

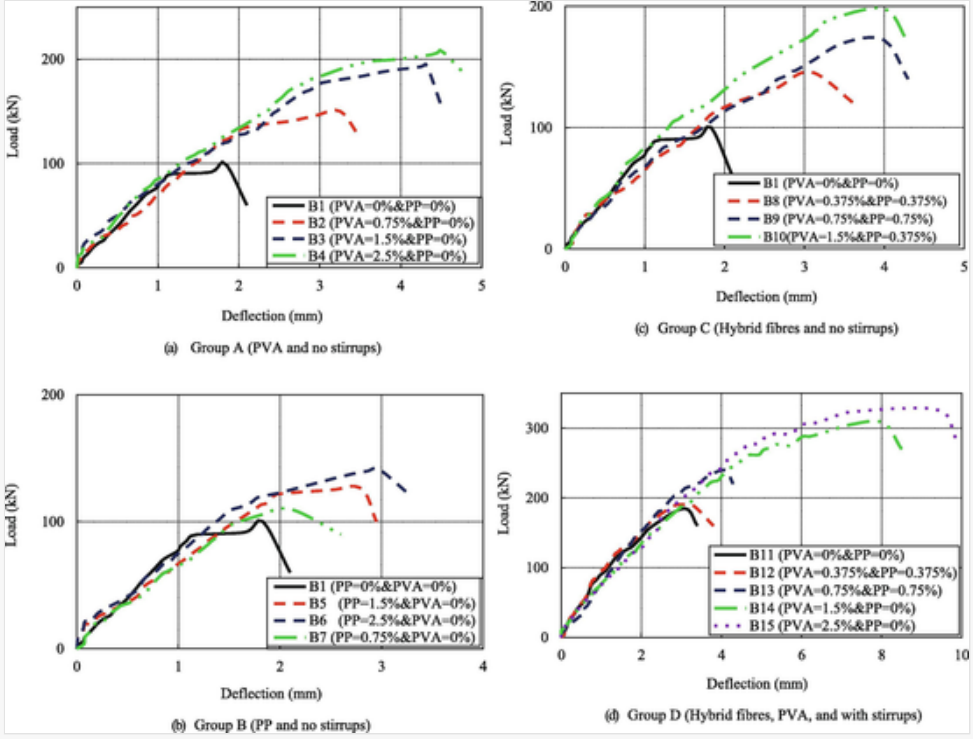


Load-deflection curves for experimentally tested beam.

**Fig 9**


a) Group A (PVA and no stirrups)




b) Group B (PP and no stirrups)


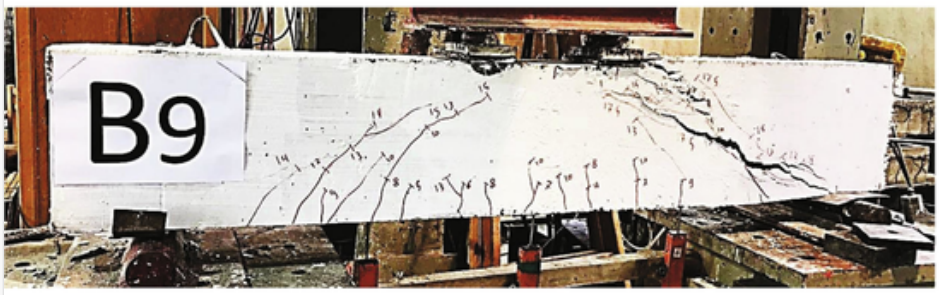



c) Group C (Hybrid fibres and no stirrups)


d) Group D (Hybrid fibres, PVA with stirrups)

Crack patterns and failure modes of experimentally tested beams 100.

### *3.1.1 Group "A" specimens (PVA only and no stirrups)*

Fig. 8 (a) shows that adding PVA to the mix resulted in a higher ultimate load and corresponding deflection of the Group A beams without stirrups compared to those of the control beam B1 to different degrees depending on the percentage of PVA. For example, specimen B1 with no PVA had an ultimate load and corresponding deflection of 100.3kN, and 1.84 mm, respectively. For specimens B2 with PVA% equals 0.75%, B3 with PVA% equals 1.5% and B4 with PVA% equals 2.5%, the ultimate loads were higher than that of specimen B1 by 50%, 94% and 107%, and their corresponding deflections were higher than that of specimen B1 by 77%, 135%, and 144.6%, respectively. Crack pattern and failure modes of the above mentioned beams are shown in Fig. 9 (a). It can be seen from the figure that B1, with no PVA fibres, exhibited brittle failure in a large diagonal shear crack at ultimate load of 100.3kN. For B2 including 0.75% PVA, the failure occurred at an ultimate load of 150 kN with a diagonal shear crack. Increasing the PVA% to 1.5 for B3, resulted in several flexural cracks as warnings, and the failure was also shear at a higher ultimate load, 194.5kN. A further increase of the PVA% to 2.5% led to a several minor flexural cracks, indicating the ductile behaviour of the beam, prior to failure due to diagonal shear at 208kN.

### *3.1.2 Group "B" specimens (PP only and no stirrups)*

Fig. 8 (b) shows the load deflection curves for Group "B" specimens with PP fibres (B5, B6, and B7) compared to that of control beam B1. It can be seen from the figure that the specimens including PP fibres showed higher ultimate loads and corresponding deflections compared with those of the control specimen B1. For example, Fig. 8 (b) shows that Specimen B5 with PP equals 1.5%, B6 with PP equals 2.5%, and B7 with PP equals 0.75% had ultimate loads and corresponding deflections of 126 kN and 2.81 mm, 142 kN and 2.97 mm, and 110 kN and 2.1 mm which are higher than those of B1 by 26% and 53%, 41% and 61%, and 10% and 14%, respectively. Crack patterns and failure modes of these beams are shown in Fig. 9 (b). It can be seen from the figure that adding PP fibres resulted in a better ductility in terms of several flexural cracks without changing the failure mode which was similar to that of B1 (diagonal shear). For example, B5 had a diagonal shear cracking load from the load application to the support at 126 kN. For B6 with PP equals 2.5%, new flexural cracks were formed all over the beam with the increment of loading and these cracks started to propagate diagonally towards the loading point as well as new diagonal cracks initiated separately away from the mid-span along the beam at 142 kN. For B7 with less PP% (0.75%), the crack pattern behaviour was better than that of B1 with minor flexural cracks until the final diagonal shear cracking at ultimate load of 110 kN.

### *3.1.3 Group C (Hybrid fibres and no stirrups)*

The load deflection curves of Group "C" specimens (B8, B9, and B10) of hybrid fibres without stirrups reinforcement were compared with that of B1 as shown in Fig. 8 (c). It can be seen from the figure that B8, B9, and B10 had ultimate loads and corresponding deflections of 145 kN and 3.08 mm, 172 kN and 3.93 mm, 198 kN and 4.02 mm which are higher than those of B1 by 45% and 67.3%, 72% and 117%, and 98% and 118%, respectively. Crack pattern and failure modes of these beams are shown in Fig. 9 (c). It can be seen from the figure that the combination of PVA and PP fibres in test beams led to a more ductile behaviour compared to the inclusion of PP

only as described Section 4.1.2. This was indicated by more vertical flexural cracks as shown in Fig. 9 (c) compared to those in Fig. 9 (b). All the beams in Group "C" failed in shear with a diagonal shear cracks similar to those in Group "B" but with more flexural cracks all over the beams compared to those observed for Group "B" (Fig. 9 (b)).

#### *3.1.4 Group d (Hybrid fibres with stirrups)*

Fig. 8 (d) shows the load deflection curves for Group "D", B11, B12, B13, B14, and B15 with hybrid fibres and stirrups. It can be seen from Fig. 8 (d) that the presence of stirrups resulted in higher ultimate loads and corresponding deflections compared with those of the beams in previously mentioned groups. It can be seen from Fig. 8 (d) that the ultimate loads and corresponding deflections of the beams including PVA and stirrups are higher than those of beams with hybrid fibres in the presence of stirrups. In addition, these values increased with increasing the PVA%. For example, the ultimate loads and corresponding deflections of specimens B14, and B15 were 308 kN and 7.93 mm, 326 kN and 9.42 mm while those of B12 and B13 with hybrid fibres were 190 kN and 3.1 mm, and 239 kN and 4.11 mm, respectively. The crack pattern and failure modes of these beams are shown in Fig. 9 (d). It can be seen from the figure that the specimens of this group which having shear reinforcement (stirrups) had ductile behaviour, in terms of small vertical flexural cracks prior to failure, compared with those of the other groups. It can be seen from the figure that B13 with hybrid fibres (0.75% PP and 0.75% PVA) had the dominance of dense flexural cracks noticed until failure compared with B11 with no fibres and B12 with less amount of hybrid fibres (0.375% PP and 0.375% PVA). Fig. 9 (d) also shows that the addition of PVA in the presence of shear reinforcement (stirrups) changed the failure mode of B14 with PVA equals 1.5% and B15 with PVA equals 2.5% from shear to combined flexure-shear with several flexural cracks throughout the beam span. Similarly, the number of cracks visible in Beam B14 are slightly more than the beam B15, thus, it can be concluded that 1.5% PVA used in B14 is close to optimum values for attaining the ductility and change of failure mode.

### 3.2 Load strain results for longitudinal reinforcement

The strains in the longitudinal tension bars reinforcement were measured as explained in Section3. The load strain relationships for longitudinal bars in studied specimens are shown in Fig. 10(a-d). It can be seen from Fig. 10(a-d) that the maximum loads recorded for longitudinal tension bars were less than the ultimate shear load at failure as recorded in Fig. 8(a-d), and the corresponding strains were all less than the yield value for high grade steel (0.0035) except for ultimate strains of B14 and B15 which were larger than yield strain. This may be attributed to the fact that the presence of stirrups in combination with PVA contributed to resist shear stresses for both of B14 and B15 which led to further action of longitudinal reinforcement in flexure which led to higher strains in longitudinal bars and, in turn, resulted in combined flexural and shear failure. That's why their longitudinal reinforcement ultimate strains exceeded the yield as a result of flexural failure. The maximum longitudinal reinforcement strains for test beams in Groups A, B, C, D were 0.0025, 0.0017, 0.002, and 0.0041 as shown in Fig. 10 (a-d).

**Fig 10**

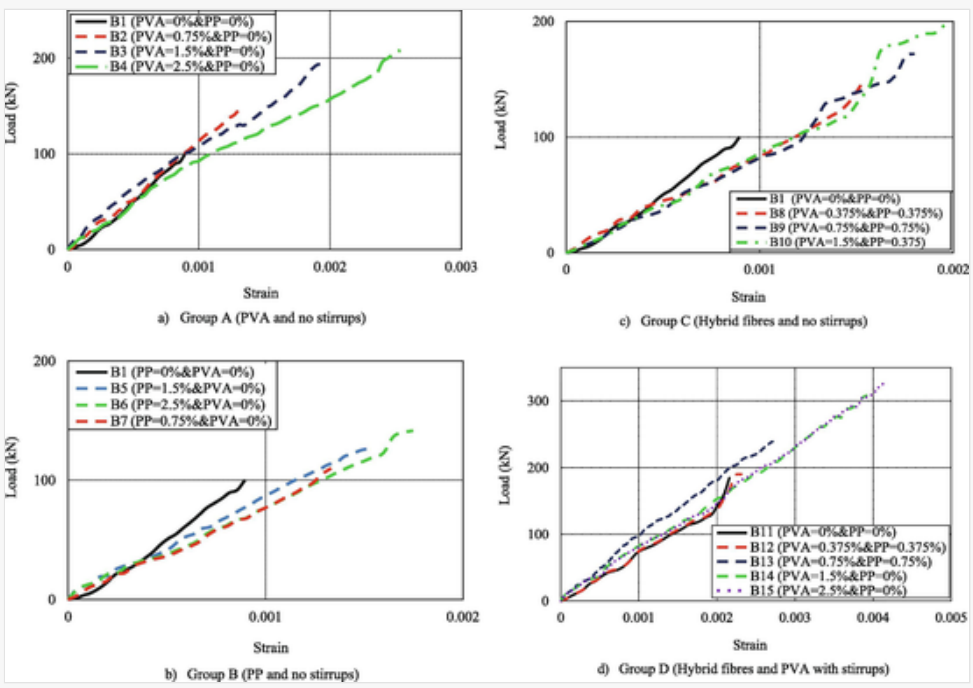


Load-strain curves for longitudinal reinforcement.

### 3.3 Discussion of the results

It can be seen from the above results that all the test beams failed in shear except for B14 and B15 which failed in flexural shear. The presence of each of PP fibres, PVA fibres, and hybrid fibres in concrete showed better ductility compared with non-fibre reinforced concrete specimen which was indicated by several flexural cracks and warnings before failure. The increase of these fibres resulted in a higher tensile strength and, in turn, a significant improvement in ductility. Similar response was also reported by Ding et al. and Smarzewski [28–30] in RC beams with shear stirrups and hybrid steel and PP fibres which was much ductile compared to those beams without fibres. The results also in coherent with the fact that the addition of hybrid fibres in beam with constant stirrup ratio transform the failure mode into ductile one [28]. In literature, hybrid steel and PP fibres are found improving the improving the flexural capacity of RC beams even in the presence of recycled aggregates [31].

PVA fibre showed a relatively greater tensile strength and recovery effect in beams as compared to PP fibre. This agrees with the results of Kang et al. [32] who reported strength improvement as a result of using PVA. Navas et al. [33] also reported that the addition of PP fibre in reinforced concrete beams improved ductility compared with their counterparts without fibres. Tran et al. [34] studied the shear behaviour of geopolymer hybrid reinforced concrete beams containing fly ash and GGBFS and reinforced with basalt fibre reinforced polymer bars as longitudinal reinforcements without stirrups. They used different fibre combinations (SF, PP, carbon fibre (CF), and PVA) to enhance the shear capacity of the beams. They found that hybridization of SF and PVA enhanced the shear capacity while the combination of PP and CF did not improve the shear strength but enhanced the ductility of the beams. It can be seen from the current investigation that the use of PP and PVA in the presence of silica fume improved both of shear strength and ductility of the studied beams.

It can also be observed that adding PVA in 1.5% (B3) and 2.5% (B4) and hybrid fibres (1.5% PVA and 0.375% PP) (B10) without shear reinforcement (stirrups) contributed towards increasing shear capacity and ductility higher than that of the control beam with stirrups (B11) (see Figs. 8-10). In addition, the combination of small amount of hybrid fibres for B13 (0.75% PP and 0.75% PVA) and stirrups reinforcement resulted in a higher shear strength and higher ductility compared to other studied beams without shear reinforcement including PVA, PP up to 2.5% or hybrid fibres (1.5% PVA and 0.375% PP). On the other hand, Pakravan et al. [22] reported that for fibre reinforced concrete ECC) beams with cement replacement by fly ash, the partial replacement of PVA fibres with PP fibres (1.5% PVA and 0.5% PP) had a positive effect on the ductility but decreased the flexural strength of the resultant ECCs. It can be argued again that the silica fume used in the current study with the hybridization of PVA and PP increased both the strength and ductility.

From the above results and discussion, the authors recommend a combination of at least hybrid fibres (0.75% PVA and 0.75% PP) and stirrups reinforcement (7.5 Ø 6 /m) to achieve adequate shear behaviour of hybrid fibre reinforced concrete beams. This combination, when adding silica fume to concrete, prevented sudden failure, improved shear strength and ductility as several small flexural cracks were formed prior to failure.

# 4 Empirical equation for predicting ultimate shear strength

An empirical equation based on the ACI-code 318-19 [35] was used in this study to predict shear strength for the studied beams in a simple way. The predicted ultimate shear strength, $V_{u,\ \mathrm{Anl}}$, was performed to be compared with the experimentally measured, $V_{u,\ \exp}$, test results. The ultimate shear strength was estimated for a single fibre reinforced concrete beam of a cross-section ($b \times t$) and containing PVA, PP or hybrid fibres in a simple way. The empirical equation used in this study for predicting ultimate shear strength of the studied beams is developed as follows:

$$V_{u,Anl} = V_c + V_{fibers} + V_s \tag{1}$$

The contribution of concrete to the shear resistance considering the aggregate interlock action ($V_a$), the resistance of compressed concrete ($V_{cc}$), and the dowel action of longitudinal bars ($V_d$) is estimated by the empirical equation of ACI-code 318–19 [35] as follows:

$$V_c = \left(0.167\sqrt{f_c} + 17\rho_s \frac{d}{a-d}\right) bd \leqslant \left(0.167\sqrt{f_c}\right) bd \tag{2}$$

The shear resistance of PVA fibres, PP fibres, and hybrid fibres ($V_{fibres}$) is contributed via the residual tensile stress ($\sigma_{et}$) acting through the diagonal tension crack. $V_{fibres}$ can be defined as follows:

$$V_{fibers} = 0.9\ \sigma_{et} bd \tag{3}$$

Shanour et al. [36] used a simplified equation for determining the residual tensile stress ($\sigma_{et}$) can be predicted as:

$$\sigma_{et} = \ 0.00772\ \frac{l_f}{\phi_f} \rho_f F_{be} \tag{4}$$

The bond efficiency of the fibre ($F_{be}$) varies from 1.0 to 1.2 depending upon fibre characteristics and ($\rho_f$) is percent by volume of the used fibres.

$\sigma_{et}$ is calculated for both PVA and PP fibre in case of specimens which contains the two types of fibres. Therefore, Eq. (4) was modified to be:

$$\alpha_{et} = \ \alpha_{et}^{PVA} + \ \alpha_{et}^{PP} \tag{5}$$

For PVA fibres: $l_f$ = 12 mm, $\phi_f$ = 39 μm and $E_f$ = 42.80 GPa;

For PP fibres: $l_f$ = 12 mm, $\phi_f$ = 18 μm and $E_f$ = 3.45 GPa;

The contribution of vertical stirrups in shear ($V_s$) can be defined as follows [26]:

$$V_s = \rho_{st} f_{ys}\ bd \tag{6}$$

Accordingly, the ultimate shear strength ($V_{u,\ Anl.}$) can be predicted from Eq. (1). The analysis procedure for calculating $Vu,\ _{num.}$ was implemented using a spreadsheet. Fig. 11 shows a comparison between the experimental and predicted ultimate shear strength. The figure shows an excellent agreement between the experimental and the ultimate shear strength results with a distinct linear relationship of a high correlation, $R^2$ = 0.9575.

**Fig 11**

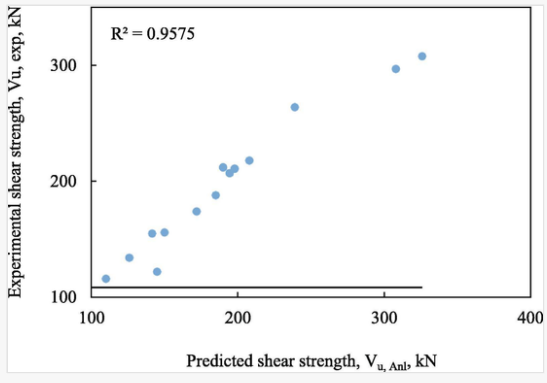


Comparison of experimental and analytical shear strength results.

# 5 Finite element analysis (FEA)

It is to note that this investigation aimed to assess the response of beams reinforced with hybrid fibres and accurately predicting the flexural response using the finite element analysis (FEA) approach by comparing with the experimental results of the flexural behaviour of 15 beams. For the FEA of hybrid reinforced RC beams using three dimensional (3D) FEA program "ATENA 3D", material properties mainly required as input parameters for the FEA, which obtained from the compressive and tensile stress–strain response. All beams modelled as a three-dimensional solid object characterized by a material model "CC3DNonLinCementitious2User" by defining user-defined material properties and material laws proposed by the researchers earlier [37,38]. CC3DNonLinCementitious2User was used to define customise fracture-plastic material model.

The reinforcement were modelled in "ATENA 3D" and the modulus of elasticity and cylindrical compressive strengths (refer to Table 6) were used as an input for material model in ATENA, while modulus of elasticity was calculated using equation 5.1−20 specified in CEB-FIP Model code 2010 [39], which is as follows:

$$E_{ci} = E_{c0} \propto_E \left( \frac{f_{ck} + 8}{10} \right)^{\frac{1}{3}} \tag{9}$$

where, $E_{ci}$ is the modulus of elasticity of concrete in MPa, $E_{c0} = 21.5 \times 10^3$ MPa, $\propto_E = 1.0$ for quartzite aggregates, $f_{ck}$ is the characteristic compressive strength of concrete in MPa based on cylindrical compressive strength.

**Table 6**

The table layout displayed in this section is not how it will appear in the final version. The representation below is solely purposed for providing corrections to the table. To preview the actual presentation of the table, please view the Proof.

Summary of the initial material input parameters for FEA and results.

| Beam ID | Beam Size (mm) | Trialed input parameters for FEA | | | | Maximum Experimental Results | | Maximum Simulated Results | |
|---|---|---|---|---|---|---|---|---|---|
| | | Mean compressive strength $(f_{cm})$ (MPa) | Modulus of elasticity $(E_{ci})$ (MPa) | Tension Function (refer to Fig. 12) | Tensile strength ($f_t$) (MPa) | Load carrying capacity (kN) | Displacement (mm) | Load carrying capacity (kN) | Displacement (mm) |
| B1 | 120 × 300 × 1800 | 44 | $37.25 \times 10^3$ | A(0, 1) | 3.62 | 100.27 | 2.25 | 100.10 | 2.2 |
| B2 | 120 × 300 × 1800 | 40 | $36.27 \times 10^3$ | A(0,1)<br>B(0.003,0.33)<br>C(0.06,0.1) | | 150 | 3.4 | 154.59 | 3.4 |
| B3 | 120 × 300 × 1800 | 40 | $36.27 \times 10^3$ | A(0,1)<br>B(0.003,0.45)<br>C(0.08,0.1) | | 194.5 | 4.5 | 195.60 | 4.6 |
| B4 | 120 × 300 × 1800 | 40 | $36.27 \times 10^3$ | A(0,1)<br>B(0.003,0.6)<br>C(0.1,0.1) | 4.68 | 208 | 4.8 | 204.00 | 4.7 |
| B5 | 120 × 300 × 1800 | 40 | $36.27 \times 10^3$ | A(0,1)<br>B(0.002,0.19)<br>C(0.02,0.05) | | 126 | 2.9 | 129.00 | 3.1 |
| B6 | 120 × 300 × 1800 | 40 | $36.27 \times 10^3$ | A(0,1)<br>B(0.002,0.3)<br>C(0.05,0.08) | | 141.6 | 3.3 | 147.20 | 3.5 |
| B7 | 120 × 300 × 1800 | 40 | $36.27 \times 10^3$ | A(0,1)<br>B(0.002,0.1)<br>C(0.01,0.02) | 4.908 | 110 | 2.6 | 112.30 | 2.4 |
| B8 | 120 × 300 × 1800 | 40 | $36.27 \times 10^3$ | A(0,1)<br>B(0.002,0.3)<br>C(0.05,0.08) | | 145 | 3.7 | 142.40 | 3.9 |
| B9 | 120 × 300 × 1800 | 40 | $36.27 \times 10^3$ | A(0,1)<br>B(0.003,0.35)<br>C(0.1,0.1) | | 172 | 4.3 | 174.80 | 4.5 |
| B10 | 120 × 300 × 1800 | 40 | $36.27 \times 10^3$ | A(0,1)<br>B(0.003,0.47)<br>C(0.09,0.1) | 3.8 | 198 | 4.2 | 199.10 | 4.4 |
| B11 | 120 × 300 × 1800 | 44 | $37.25 \times 10^3$ | A(0, 1) | | 185 | 3.5 | 188.30 | 3.7 |
| B12 | 120 × 300 × 1800 | 40 | $36.27 \times 10^3$ | A(0,1)<br>B(0.003,0.42)<br>C(0.07,0.1) | | 190 | 3.8 | 192.50 | 4.1 |
| B13 | 120 × 300 × 1800 | 40 | $36.27 \times 10^3$ | A(0,1)<br>B(0.003,0.35)<br>C(0.1,0.1) | 4.95 | 239 | 4.3 | 242.30 | 4.5 |
| B14 | 120 × 300 × 1800 | 40 | $36.27 \times 10^3$ | A(0,1)<br>B(0.003,0.45)<br>C(0.08,0.1) | | 308 | 8.6 | 295.00 | 8.8 |
| B15 | 120 × 300 × 1800 | 40 | $36.27 \times 10^3$ | A(0,1)<br>B(0.003,0.6)<br>C(0.1,0.1) | | 326 | 9.5 | 313.77 | 9.7 |

In order to obtain tensile parameters as tensile strength and tension function (refer to Fig. 12 and Table 6), the response of direct tensile test is required. Unfortunately, the test was not performed due to complexity of test sample. The following steps were taken to obtain the input parameters as also suggested by ATENA Manual [40]:

**Fig 12**

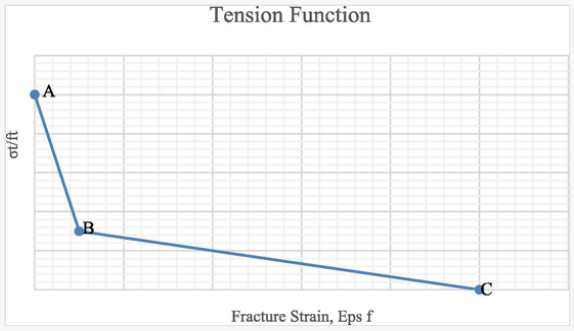


Generalised Tension Function used in Atena 3D.

1. Initial setup of the tensile parameters (tensile strength, tensile function),

2. After analysis, comparison of load–displacement diagram with experimental test,

3. Once the Load-displacement diagram was close enough, the determination of tensile parameters was completed; the input parameters were trialled several times in order to achieve better results.

All beams modelled on a full-scale up to point of symmetry by using typical dimension of 120 × 300 × 900 mm, as shown in Fig. 12. The beams were typically simply supported at the bottom on steel plates, and the displacement in the direction of the beam length (i.e., X = free, Y = free, and Z = fixed) was set as zero (refer to Fig. 13). The "brick" element type finite element mesh was created as a three-dimensional cubical structure comprised of a cubical structure of 20 × 20 × 20 mm, as shown in Fig. 14.

**Fig 13**

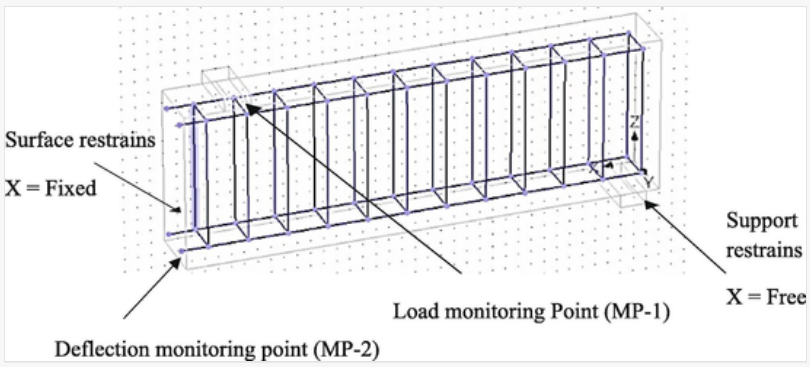


FEA beam support restrains and monitoring point detail.

**Fig 14**

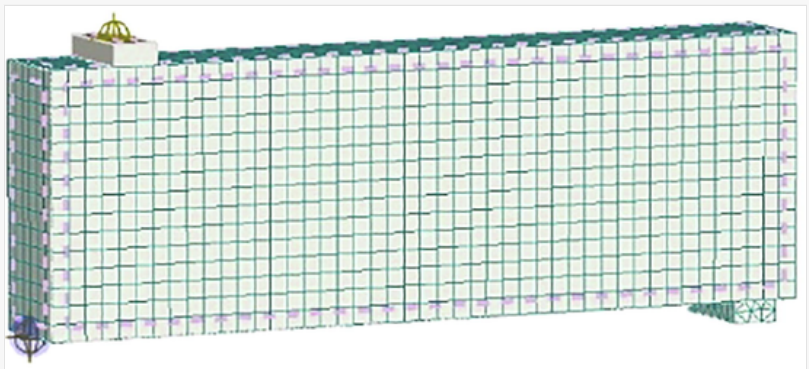

Finite element models of beams using ATENA 3D program.

The basis for selecting this mesh type was the literature presented in [41], which recommends this mesh type for better analysis results quality considering the speed and memory requirements. Fig. 14 shows the generated FE mesh. The support restrained modelled as a typical roller and hinged; that is, there was a vertical and horizontal restraining movement of modelled Beam. The material properties, as given in Table 6, were assigned to the beams, which included cylindrical compressive strength, tensile strength, modulus of elasticity, and fracture energy. The results of FE analysis, that is, load and vertical displacement in the generated model, were monitored to have information about the structure's state after applying prescribed loadings. The information collected by monitoring the predefined two monitoring points (MP) (refer to Fig. 13) is as follows:

1. The first MP-1 was marked at the top of the loading rod at mid-span of the Beam to acquire the maximum load attained by the Beam before the failure.
2. The second MP-2 was marked in the middle of the Beam near its bottom surface at mid-span of the Beam, where the largest vertical displacements were expected.

There was a smeared crack approach adopted for the fracture mechanism. A typical critical stress location failure pattern in the analyzed Beam, representative of all beams, is shown in Fig. 15. Three types of results were obtained from 3D nonlinear FE analysis using ATENA 3D:

1. Maximum load (MP-1) versus deflection (MP-2)
2. Failure mode (or crack pattern at failure), and
3. Post-peak response of the concrete in the absence and presence of the shear stirrups and Fibres

Fig 15

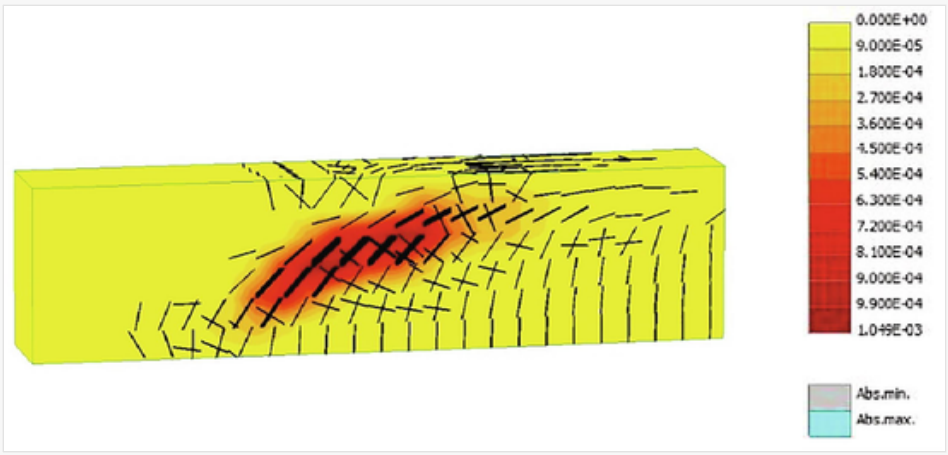


A typical crack pattern of a simulated beam at failure in ATENA 3D program.

The comparison of FEA results with the experimental and mathematical results is presented in Table 6, which shows that the similarity of FEA results in terms of load and deflection with the experimental results is more than 90%. This confirms that the 3D finite element modeling is significantly accurate. The comparison of load–deflection curves obtained from the ATENA 3D program resulted from FEA, with the experimental results. Fig. 16 shows the comparison of the simulated versus experimental load–deflection curves for all specimens.

Fig 16

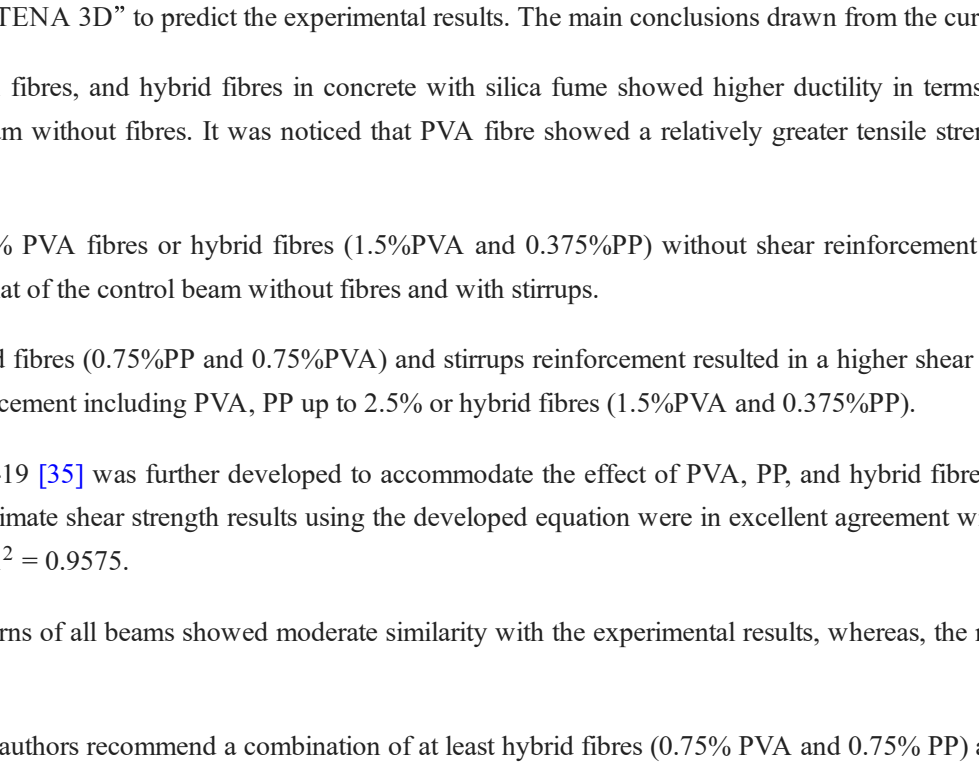


Load-deflection response of all beams and their FEM Simulations.

## 6 Conclusions and recommendations

Fifteen fibre reinforced concrete beams containing 15% silica fume, shear span to depth ratio (a/d = 2.25) and different percentages of PVA, PP, and hybrid fibres were experimentally tested. In addition, an empirical equation based on ACI 318-19 [35] was used to predict shear strength. Moreover, the tested beams were modelled using the three dimensional (3D) FEA program “ATENA 3D” to predict the experimental results. The main conclusions drawn from the current study are listed below.

The presence of each of PP fibres, PVA fibres, and hybrid fibres in concrete with silica fume showed higher ductility in terms of several flexural cracks and warnings before failure compared with control beam without fibres. It was noticed that PVA fibre showed a relatively greater tensile strength and recovery effect compared to PP fibre.

It was found that adding more than 1.5% PVA fibres or hybrid fibres (1.5%PVA and 0.375%PP) without shear reinforcement (stirrups) contributed towards increasing shear capacity and ductility higher than that of the control beam without fibres and with stirrups.

A combination of small amount of hybrid fibres (0.75%PP and 0.75%PVA) and stirrups reinforcement resulted in a higher shear strength and higher ductility compared to other studied beams without shear reinforcement including PVA, PP up to 2.5% or hybrid fibres (1.5%PVA and 0.375%PP).

A proposed equation based on ACI 318-19 [35] was further developed to accommodate the effect of PVA, PP, and hybrid fibres to predict shear strength for the studied beams in a simple way. The estimated ultimate shear strength results using the developed equation were in excellent agreement with the experimental results with a distinct linear relationship of a high correlation, $R^2 = 0.9575$.

In general, the FEA results of crack patterns of all beams showed moderate similarity with the experimental results, whereas, the maximum load, load versus deflection are very close to experimental results.

From the results of this investigation, the authors recommend a combination of at least hybrid fibres (0.75% PVA and 0.75% PP) and stirrups reinforcement (7.5 Ø 6 /m) to achieve adequate shear behaviour of hybrid fibre reinforced concrete beams. This combination prevented sudden failure and improved the ductility as several small flexural cracks were formed prior to failure.

In this study, limited *a/d* ratios have been investigated; therefore, a further investigation, specifically at *a/d* ratio of 2 and 6, is further needed to be investigated for PVA-FRC. Therefore, it is recommended to investigate the effect of an extensive range of shear span-depth (*a/d*) ratio on the flexural strength of PVA-FRC and FRCs containing other fibre types.

## Declaration of Competing Interest

The authors declare that they have no known competing financial interests or personal relationships that could have appeared to influence the work reported in this paper.


## Acknowledgement

The authors wish to acknowledge the staff and technicians of Concrete Research Laboratory at Faculty of Engineering, Cairo University for their help and support throughout the program of the experimental work.


## References




[1] Shi F., Pham T.M., Hao H., Hao Y. Post-cracking behaviour of basalt and macro polypropylene hybrid fibre reinforced concrete with different compressive strengths. Constr Build Mater 2020;262:120108.

[2] Chen Y., Qiao P. Crack growth resistance of hybrid fiber-reinforced cement matrix composites. J Aerosp Eng 2011;24(2):154–161.

[3] Khan M., Cao M., Ali M. Cracking behaviour and constitutive modelling of hybrid fibre reinforced concrete. J Build Eng 2020;30:101272.

[4] Soe K.T., Zhang Y., Zhang L. Material properties of a new hybrid fibre-reinforced engineered cementitious composite. Constr Build Mater 2013;43:399–407.

[5] Kim D.J., Park S.H., Ryu G.S., Koh K.T. Comparative flexural behavior of hybrid ultra high performance fiber reinforced concrete with different macro fibers. Constr Build Mater 2011;25(11):4144–4155.

[6] Tian H., Zhang Y., Ye L., Yang C. Mechanical behaviours of green hybrid fibre-reinforced cementitious composites. Constr Build Mater 2015;95:152–163.

[7] Asok G, George S. Investigation on hybrid concrete using steel and polypropylene fiber. Int J New Technol Res 2016;2(5)

[8] Sukontasukkul P. Tensile behaviour of hybrid fibre-reinforced concrete. Adv Cem Res 2004;16(3):115–122.

[9] Li B., Chi Y., Xu L., Shi Y., Li C. Experimental investigation on the flexural behavior of steel-polypropylene hybrid fiber reinforced concrete. Constr Build Mater 2018;191:80–94.

[10] Stroeven P., Shui Z., Qian C., Cheng Y. Properties of carbon-steel and polypropylene-steel hybrid fiber concrete in low-volume fraction range. Special Publication 2001;200:713–732.

[11] KM, AF, Varghese S. Behavioral study of steel fiber and polypropylene fiber reinforced concrete. Int J Res Eng Technol 2014;2(10):17–24

[12] Hou X., Abid M., Zheng W., Hussain R.R. Effects of temperature and stress on creep behavior of PP and hybrid fiber reinforced reactive powder concrete. Int J Concr Struct Mater 2019;13(1):45.

[13] Smarzewski P. Flexural toughness of high-performance concrete with basalt and polypropylene short fibres. Adv Civ Eng 2018;2018.

[14] Wang D., Ju Y., Shen H., Xu L. Mechanical properties of high performance concrete reinforced with basalt fiber and polypropylene fiber. Constr Build Mater 2019;197:464–473.

[15] Yan P., Chen B., Afgan S., Haque M.A., Wu M., Han J. Experimental research on ductility enhancement of ultra-high performance concrete incorporation with basalt fibre, polypropylene fibre and glass fibre. Constr Build Mater 2021;279:122489.

[16] Pakravan H.R., Latifi M., Jamshidi M. Ductility improvement of cementitious composites reinforced with polyvinyl alcohol-polypropylene hybrid fibers. J Ind Text 2016;45(5):637–651.

[17] Pakravan H., Jamshidi M., Latifi M. The effect of hybridization and geometry of polypropylene fibers on engineered cementitious composites reinforced by polyvinyl alcohol fibers. J Compos Mater 2016;50(8):1007–1020.

[18] Feng J., Sun W., Zhai H., Wang L., Dong H., Wu Q. Experimental study on hybrid effect evaluation of fiber reinforced concrete subjected to drop weight impacts. Materials 2018;11(12):2563.

[19] Ismail M.K., Hassan A.A. Influence of fibre type on the shear behaviour of engineered cementitious composite beams. Mag Concr Res 2019;1–12.

[20] Corinaldesi V., Moriconi G. Mechanical and thermal evaluation of Ultra High Performance Fiber Reinforced Concretes for engineering applications. Constr Build Mater 2012;26(1):289.

[21] Empelmann M, Teutsch M, Steven G. Improvement of the Post Fracture Behaviour of UHPC by Fibres. In: Editor “Book Improvement of the Post Fracture Behaviour of UHPC by Fibres”, kassel university press GmbH; 2008. p. 177

[22] Granju J.-L., Balouch S.U. Corrosion of steel fibre reinforced concrete from the cracks. Cem Concr Res 2005;35(3):572.

[23] 2004/1-197EN, Cement; Composition, specifications and conformity criteria; 2004

[24] ASTM C1240, Standard specification for silica fume used in cementitious mixtures; 2003

[25] A1 TE. Admixtures for concrete, mortar and grout–Part 2: Concrete admixtures–Definitions, requirements, conformity, marking and labelling; 2013

[26] EN 12350-2 (2009) Testing fresh concrete. Slump-test; 2009

[27] EN 206-1 (2006) Concrete-part 1: specification, performance, production and conformity, CEN; 2006

[28] Ding Y., You Z., Jalali S. Hybrid fiber influence on strength and toughness of RC beams. Compos Struct 2010;92(9):2083–2089.

[29] Smarzewski P. Hybrid fibres as shear reinforcement in high-performance concrete beams with and without openings. Appl Sci 2018;8(11):2070.

[30] Smarzewski P. Analysis of failure mechanics in hybrid fibre-reinforced high-performance concrete deep beams with and without openings. Materials 2019;12(1):101.

[31] Karimipour A, Ghalehnovi M. Comparison of the effect of the steel and polypropylene fibres on the flexural behaviour of recycled aggregate concrete beams. In: Editor “Book Comparison of the effect of the steel and polypropylene fibres on the flexural behaviour of recycled aggregate concrete beams”, Elsevier; 2021. p. 129-146

[32] Kang C., Huh J., Tran Q.H., Kwak K. Evaluation of self-healing performance of PE and PVA concrete using flexural test. Adv Mater Sci Eng 2018;2018.

[33] Navas F.O., Navarro-Gregori J., Herdocia G.L., Serna P., Cuenca E. An experimental study on the shear behaviour of reinforced concrete beams with macro-synthetic fibres. Constr Build Mater 2018;169:888–899.

[34] Tran T.T., Pham T.M., Hao H. Effect of hybrid fibers on shear behaviour of geopolymer concrete beams reinforced by basalt fiber reinforced polymer (BFRP) bars without stirrups. Compos Struct 2020;112236.

[35] ACI 318-19, Building code requirements for structural concrete, American Concrete Institute; 2019

[36] Shanour A.S., Said M., Arafa A.I., Maher A. Flexural performance of concrete beams containing engineered cementitious composites. Constr Build Mater 2018;180:23–34.

[37] Ayub T., Khan S.U., Ayub A. Analytical model for the compressive stress–strain behavior of PVA-FRC. Constr Build Mater 2019;214:581–593.

[38] Khan S.U., Ayub T. Modelling of the pre and post-cracking response of the PVA fibre reinforced concrete subjected to direct tension. Constr Build Mater 2016;120:540–557.

[39] fib Bulletin 55, “CEB-FIP Model Code 2010”, International Federation for Structural Concrete (fib); 2010

[40] Sajdlová T. ATENA Program Documentation, Part 4-9“; 2015

[41] Cervenka V, Jendele L, Cervenka J. ATENA program documentation part 1 theory, Cervenka Consulting, Prague, vol. 231; 2007